



HAL
open science

Impact of turbulence on power production by a free-stream tidal turbine in real sea conditions

Alexei Sentchev, Maxime Thiébaud, François Schmitt

► To cite this version:

Alexei Sentchev, Maxime Thiébaud, François Schmitt. Impact of turbulence on power production by a free-stream tidal turbine in real sea conditions. *Renewable Energy*, 2020, 147 (Part 1), pp.1932-1940. 10.1016/j.renene.2019.09.136 . hal-03085657

HAL Id: hal-03085657

<https://hal.science/hal-03085657>

Submitted on 21 Dec 2020

HAL is a multi-disciplinary open access archive for the deposit and dissemination of scientific research documents, whether they are published or not. The documents may come from teaching and research institutions in France or abroad, or from public or private research centers.

L'archive ouverte pluridisciplinaire **HAL**, est destinée au dépôt et à la diffusion de documents scientifiques de niveau recherche, publiés ou non, émanant des établissements d'enseignement et de recherche français ou étrangers, des laboratoires publics ou privés.

1 **Impact of turbulence on power production by a free-stream tidal**
2 **turbine in real sea conditions**

3
4
5 **Alexei Sentchev*¹, Maxime Thiébaud^{1,2} and François G. Schmitt¹**

6
7 (1) *Univ. Littoral Côte d'Opale, Univ. Lille, CNRS, UMR 8187, LOG,*
8 *Laboratoire d'Océanologie et de Géosciences, Wimereux, France*

9
10 (2) *France Énergies Marines, Technopôle Brest Iroise, 525 Avenue de Rochon, 29280 Plouzané,*
11 *France*

12 (*) *Corresponding author : alexei.sentchev@univ-littoral.fr*

13 *Phone : +33 3 21 99 64 17 Fax : + 33 3 21 99 64 01*

14
15 **Abstract**

16 An experiment was performed to study the power production by a Darrieus type turbine of the Dutch
17 company Water2Energy in a tidal estuary. Advanced instrumentation packages, including mechanical
18 sensors, acoustic Doppler current profiler (ADCP), and velocimeter (ADV), were implemented to
19 measure the tidal current velocities in the approaching flow, to estimate the turbine performance and to
20 assess the effect of turbulence on power production. The optimal performance was found to be
21 relatively high ($C_p \sim 0.4$). Analysis of the power time history revealed a large increase in magnitude of
22 power fluctuations caused by turbulence as the flow velocity increases between 1 and 1.2 m/s.
23 Turbulence intensity does not alone capture quantitative changes in the turbulent regime of the real
24 flow. The standard deviation of velocity fluctuations was preferred in assessing the effect of
25 turbulence on power production. Assessing the scaling properties of the turbulence, such as dissipation
26 rate, ε , the integral lengthscale, L , helped to understand how the turbulence is spatially organized with
27 respect to turbine dimensions. The magnitude of power fluctuations was found to be proportional to L
28 and the strongest impact of turbulence on power generation is achieved when the size of turbulent
29 eddies matches the turbine size.

30
31 **Keywords:** Tidal stream energy, Turbine performance, Turbulence, Velocity measurements.
32
33

34 **1. Introduction**

35 Tidal stream energy is growing rapidly in interest as countries look for ways to generate
36 electricity without relying on fossil fuels. In comparison to other sources of renewable energy, tidal
37 stream energy is accurately predictable and the social acceptance level is higher due to a reduced
38 visual impact.

39 Whilst the major characteristics of the mean tidal flow (speed, direction, current magnitude
40 asymmetry, etc) are relatively simple to measure (e.g., Guerra and Thomson, 2017; Thomson et al.,
41 2010; Thiébaud and Sentchev, 2016, 2017), much less is known about turbulence. This is indicative of
42 the inherent technical difficulties (i.e., sensor movement, limited sampling rate) in acquiring
43 measurements of turbulent motions in fast moving currents (e.g., Milne et al., 2013).

44 During the last decade, with increasing deployment of Tidal Energy Converters (TECs)
45 prototypes in many countries, large effects of turbulence on turbine functioning and performance have
46 been reported (MacEnri et al., 2013; Li et al., 2014; Verbeek et al., 2017). The design of TECs can be
47 optimized in response to results revealed during trials. Until recently, the technology optimization,
48 quality and reliability improvements of TECs were obtained by both experimental research in flume
49 tanks (e.g., Bahaj et al., 2007; Mycek et al., 2014; Chamorro et al., 2013) and modeling (e.g., Batten et
50 al., 2008, 2013; Pinon et al., 2012; Li and Calisal, 2010; Churchfield et al., 2013). For example, the
51 most sophisticated Large Eddy Simulations, performed by Churchfield et al. (2013), yield a detailed
52 time-dependent structure of the turbulent flow and showed that the way in which the turbulent flow is
53 simulated greatly affects the predicted power production by the array of turbines.

54 As advances in numerical simulations support the increased confidence in prediction of turbine
55 performance, the need remains to establish experimental verification of modeling results. Important
56 results characterizing the functioning of a horizontal axis turbine and an array of turbines under a
57 range of flow conditions have been obtained from device testing in flume tanks. These tests have
58 provided valuable data at the small experimental scale and, in particular, provided indications on how
59 current speed and current/wave interaction can affect the power production by the turbine (e.g., Tatum
60 et al., 2016; Pinon et al., 2012). Other experimental works highlighted the impact of turbulence on
61 turbine performance (e.g. Bahaj and L. E. Myers, 2013; Blackmore et al., 2016; Medina et al., 2017).

62 However, real life deployments of full-scale prototypes provide a great opportunity for detailed
63 assessment of the tidal device performance. The number of scientific publications reporting the results
64 of full-scale device trials is scarce. Experimental approach developed by McNaughton et al. (2015)
65 allowed assessing the performance of Alstom 1 MW tidal turbine in real sea conditions at the
66 European Marine Energy Centre in Orkney. The results showed a large sensitivity of the turbine
67 performance to the shape of velocity profile and turbulence level in tidal flow. Assessment of the
68 MCT SeaGen 1.2 MW tidal energy converter performed by MacEnri et al. (2013) came to similar
69 conclusions. In particular, it revealed a large effect of turbulence strength, generated at high current

70 speed, on the flicker level (i.e., the level of rapid fluctuations in the voltage of the power supply).
71 Jeffcoate et al. (2015) investigated the performance of a 1/10 scale tidal turbine (1.5 m diameter) in
72 both steady state and real sea flow conditions at the experimental site in Strangford Narrows (UK). A
73 clear decrease and strong variations of the TEC performance in turbulent tidal flow were documented.
74 However turbulent properties of the flow at site were not estimated and a link with the power
75 production was not established. A two-year experimental study of a full scale TEC prototype
76 conducted at a demonstration site at Uldolmok (South Korea) demonstrated that the TEC's integrity is
77 significantly affected by short-term inflow disturbances such as natural turbulence and vortex
78 shedding. Moreover it was highlighted that turbulent instabilities in flow regime might ultimately
79 contribute to a catastrophic failure through an excitation of the system resonance (Li et al., 2014).

80 The purpose of this paper is twofold. First, the study aims to provide an estimated performance of
81 a vertical axis (Darrieus type) tidal turbine. Insights into methodology and practice of tidal stream
82 turbine testing in real turbulent flow are presented. The second objective aims to clarify how the
83 turbulence in evolving tidal stream affects power production. The study attempts to identify the most
84 relevant metrics of turbulence which help to better understand and quantify changes in turbulence
85 regime in the real tidal flow as well as the relationship with power production.

86

87 **2. Materials and methods**

88 **2.1 Tidal current turbine**

89 The Darrieus type vertical axis tidal turbine (VATT) was designed and manufactured by the Dutch
90 company Water2Energy B.V. (Ltd), based in Heusden (NL). The turbine rotor, equipped with four
91 vertical blades (Fig. 1), employs a hydrodynamic lift principle that causes the blades to move
92 proportionately faster than the surrounding water. A fairly low rotation speed, ranging from 5 to 45
93 rotations per minute (rpm), does not have a significant influence on the movement of fish and other
94 marine biological species. A new generation turbine, tested in the Sea Scheldt in autumn 2014 and
95 called Dragonfly II, was fitted with an improved pitch control of the foils.

96 The turbine was mounted on a floating frame, featuring two floaters and cross beams shown in
97 Fig. 1. It was positioned in the 2-m thick uppermost surface layer in natural tidal flow. The elements
98 rotating in the water (blades, arms) have the dimensions: 2 m rotor diameter and 1.5 m blade length,
99 thus the area swept by the blades was 3 m². The mechanical and electrical components of the turbine
100 were located above the waterline, increasing the lifespan and enabling easy installation and
101 maintenance. During the turbine test runs, the output power, rotation speed, and torque were
102 continuously recorded at 100 Hz by the data acquisition unit mounted on the platform next to the
103 turbine. The cut-in speed was about 0.5 m/s. The cut-off velocity was not specified by the
104 manufacturer. The maximum power generation was expected to be about 5 kW. When the turbine is
105 running, the electric power is used to charge the batteries and to supply any A/C loads attached. If the

106 batteries are fully charged and the A/C load is lower than that produced by the turbine, the turbine
107 slightly speeds down until the power output and loads are balanced. With the pitch control of the foils,
108 the efficiency is expected to be high, of the order of 0.45 to 0.5.

109

110 **2.2 Experimental site and tidal flow regime**

111 The tidal turbine was tested in real sea conditions in a tidal estuary (the Sea Scheldt) at an
112 experimental site located in Temse, west of Antwerp (Belgium). A floating pontoon (3m x 39 m),
113 oriented in the streamwise direction, was installed in the middle of the Sea Scheldt between two piles,
114 embedded in the river bed (Fig. 1 lower panel). The mean depth and the river width were
115 approximately 10 m and 300 m. The turbine was installed alongside the pontoon during a six-week
116 period from October 20, to December 11, 2014. More details on the trials conducted in the Sea Scheldt
117 can be found in (Goormans et al., 2016).

118 The flow regime in the estuary is essentially governed by tides of semi-diurnal period with a
119 slight fortnight modulation. At site location, the water level varies between 7 and 13 m providing a
120 mean tidal range of 6 m. The tidal wave propagates from roughly East to West along the main river
121 axis (Fig. 2). During a tidal cycle, the current vector draws an ellipse (Fig. 3) whose semi-major axes
122 match the flood (red dots) and ebb (blue dots) current direction. At rising tide, the mean flow direction
123 in the surface layer 2-m thick is $\sim 167^\circ$ (with respect to East) and referred to as flood flow direction. At
124 falling tide, the ebb flow direction is -7° revealing a slight misalignment with flood flow (Fig. 3). The
125 current vector rotation is counter-clockwise due to bottom friction which affects the water movement
126 at all depth levels.

127 The salinity at site is close to zero in the whole water column due to a strong mixing and large
128 distance from the sea. The weather conditions were calm, during the targeted period, with low wind
129 and insignificant wave height (< 0.2 m).

130

131 **2.3 Velocity measurements**

132 The tidal currents were measured by a downward-looking 1.2-MHz RDI Workhorse Sentinel
133 acoustic Doppler current profiler (ADCP) and a velocimeter (ADV) Vector from Nortek. Both
134 instruments were mounted on a steel beam extending out from the side of the pontoon and positioned
135 upstream in front of the turbine (Fig. 1 lower panel). ADV was aligned with the middle line of the
136 turbine whereas ADCP was out of line by approximately 1 m. Both ADV and ADCP were spaced from
137 the tidal turbine by a distance of $\sim 2D = 4$ m, D being the turbine diameter.

138 The ADCP recorded current velocity during several tidal periods of turbine test runs. The
139 instrument was set to operate at a pinging rate of 1 Hz recording velocity profiles every second. Each
140 ping of velocity profiling was composed of three sub-pings averaged within 1-second interval
141 providing velocity error of 0.04 m/s, according to manufacturer documentation and software.
142 Velocities were recorded in beam coordinates with 0.25 m vertical resolution (bin size), starting from

143 0.8 m below the surface (midpoint of the first bin). ADCP velocities were used for tidal flow
144 characterization, evaluation of the kinetic power available in the flow and comparison with velocities
145 measured by ADV. Three deployments were carried out at the test site using identical configuration.
146 The longest period of data acquisition lasted 11 tidal cycles (7-11 November 2014).

147 The ADV installed next to the ADCP, was recording 3 components of the flow velocity (east,
148 north and vertical) at 16 Hz at ~1 m depth which corresponded to the second ADCP bin. The
149 installation on the steel beam, tightly fixed to the pontoon, ensured a good stability of instruments. For
150 the range of velocity variations encountered at site and under similar calm wave climate conditions,
151 Richard et al. (2013) evaluated the Doppler noise of ADV measurements as 0.03-0.04 m/s. The
152 Doppler noise in ADCP measurements was estimated following a technique proposed by Thomson et
153 al. (2012). The velocity standard deviations for ADCP and ADV were compared and the Doppler noise
154 in ADCP data was found to be 0.06 m/s at flood and 0.05 m/s at ebb flow respectively. Before
155 removing the Doppler noise, ADCP velocity standard deviations were almost 60% larger than that
156 derived from ADV.

157 A low eccentricity of the tidal current ellipse allowed taking into account only the streamwise
158 velocity component for characterization of tidal motions in the estuary. Therefore horizontal velocity
159 components recorded by ADCP were projected on along- and cross-stream axes (x and y) of the river
160 (Fig. 2). The projection angle (13° clockwise) matches the orientation of the tidal current ellipse in the
161 surface 2-m thick layer on flood tide (Fig. 3). Time series of the streamwise velocity, referred to as u
162 component, and spanwise velocity (v component), derived from both ADCP and ADV, were thus
163 generated for further analysis.

164 The streamwise velocities, recorded by ADCP during five flood flow intervals (Fig. 4), were
165 used to estimate the turbine performance, whereas ADV data were used for assessing the turbulent
166 properties of the tidal flow. We had a limited length of ADV velocity time series, a total of 24 hours
167 during the trial period in November. Comparison of 10 min averaged velocities, derived from ADCP
168 and ADV records, showed a good overall agreement (Fig. 8a) with relative error less than 6%.

169

170 **2.4 Analysis techniques and metrics used for turbulence characterization**

171 Standard statistical parameters were estimated using the velocity time series provided by ADCP:
172 the time mean, the maximum and the standard deviation of velocity variations. Velocity values
173 averaged over one-minute time intervals, were used to evaluate the turbine performance, whereas
174 turbulent properties of the flow were quantified by using high frequency ADV measurements.

175 The turbulence intensity, often referred to as turbulence level, is defined as:

176
$$I = \frac{\sigma}{U},$$

177 where U is the mean velocity computed from the three mean velocity components U_x , U_y and U_z as:

$$178 \quad U \equiv \sqrt{U_x^2 + U_y^2 + U_z^2}, \text{ and } \sigma \equiv \sqrt{\frac{1}{3}(\sigma_x^2 + \sigma_y^2 + \sigma_z^2)}$$

is the standard deviation of the mean velocity.

179 This metric has been shown to correlate with the extreme loads exerted on turbine blades and is
180 assumed to be a source of fatigue.

181 The dissipation rate, ε , of the turbulent kinetic energy is estimated from the power spectrum
182 density (PSD) of velocity, $E(k)$, assuming the Kolmogorov relationship of the local isotropic
183 turbulence (Frish, 1995; Pope, 2000):

$$184 \quad E(k) = C\varepsilon^{2/3}k^{-5/3},$$

185 where C is the Kolmogorov's constant ($C = 1.5$) and k is the wavenumber. Using Taylor's assumption
186 of frozen turbulence, the frequency f and wavenumber k can be related to the mean velocity U such as:
187 $k = 2\pi f/U$. Thus, the dissipation rate can be estimated from the power spectrum as (Thomson et al.,
188 2012):

$$189 \quad \varepsilon = \left(\frac{C_0}{C}\right)^{3/2} \left(\frac{2\pi}{U}\right)^{5/2},$$

190 where C_0 accounts for the height of the PSD slope which best fits the spectrum in the inertial
191 subrange.

192 The value of ε is used to estimate three other important scaling properties: the integral lengthscale
193 L , thought as the size of the most energetic turbulent eddies, the Kolmogorov dissipation scale η , and
194 the Taylor lengthscale λ defined by (Pope, 2000):

$$195 \quad L = \frac{\sigma_u^3}{\varepsilon},$$

$$196 \quad \eta = \left(\frac{\nu^3}{\varepsilon}\right)^{1/4},$$

197 and

$$198 \quad \lambda = \sqrt{\frac{15\nu}{\varepsilon}}\sigma_u.$$

199 where ν is the kinematic viscosity of water ($\nu = 1.5 \times 10^{-6} \text{ m}^2/\text{s}$). Finally, two Reynolds numbers based
200 on the Taylor lengthscale λ and on the water depth h were estimated according to:

$$201 \quad Re_\lambda = \frac{\sigma_u \lambda}{\nu} \qquad Re = \frac{U h}{\nu}.$$

202

203 3. Results

204 3.1 Turbine performance assessment in real flow conditions

205 A typical cycle of tidal flow evolution is shown in Fig. 4a. On average, the streamwise
206 velocity, u , exceeds the spanwise velocity, v , by an order of magnitude (Fig. 4a). The duration of the

207 flood and ebb flow periods were found to be sensibly different – 7 and 5.5 hours respectively. After
208 the current reversal (CR) of low water (LW), the tidal current velocity evolves from 0.8 m/s to -0.8
209 m/s in less than 1 hour, revealing very short slack water duration.

210 The imbalance between flood and ebb flow, clearly identified in Fig. 3 and known as current
211 magnitude asymmetry a , is defined as the ratio of the mean velocity during flood tide to the mean
212 velocity during ebb tide: $a = \langle u_{\text{flood}} \rangle / \langle u_{\text{ebb}} \rangle$. This is a relevant metric allowing a more realistic
213 estimate of tidal stream resource at site (e.g., Neill et al., 2014; Thiébaud and Sentchev, 2017).

214 On average, a was found to be 0.75 during the survey period. In the surface layer, the mean ebb
215 tide velocity is above 1 m/s whereas during flood tide it is below 0.8 m/s. Such a difference is related
216 to a particular shape of the velocity curve with a significant saddle point during the flood phase of the
217 tide. The maximum velocities during the flood and ebb tide were observed at LW and HW
218 respectively.

219 The performance of the W2E tidal turbine is characterized by estimating the power coefficient,
220 C_p , defined as a ratio of the output power P generated by the turbine to the kinetic energy in the
221 approaching flow passing the area S swept by the blades:

$$C_p = \frac{P}{(1/2)\rho S u^3}$$

222 Here, ρ is the water density, and u is the streamwise velocity of incoming flow. Velocities
223 recorded by ADCP 0.8 m below the surface, i.e. at the mid-depth of the operating turbine, are assumed
224 to account for space averaged values. This assumption is realistic since the velocity profiles show a
225 slight linear variation in the uppermost surface layer during the whole cycle of operation (Fig. 5).

226 The power coefficient C_p was assessed using u velocity time series that were recorded during
227 three flood tide periods (on November 7, 8, and 9) on a 1-minute average. The output power was also
228 1-minute averaged and synchronized with the velocity measurements. Only power time series recorded
229 during flood flow, occurring in the afternoon of each date, were subsequently used in analysis as they
230 provided better quality power data and larger record length (Fig. 4b). During two night trials, the
231 power records showed abnormal variations which we cannot explain. These data were not used in the
232 analysis. The resulting distribution of C_p estimates is shown in Fig. 6a.

233 The optimum efficiency was achieved for a flow velocity close to 1.2 m/s, yielding $C_p \sim 0.42$. For
234 lower current velocity values, 0.85 - 1 m/s, the efficiency falls to 0.30. The spreading of the power
235 coefficient throughout the tidal velocity range is caused by variations of the torque which, in turn,
236 result from unsteady loading exerted on the blades by tidal flow instabilities.

237 By taking into account variations in turbine rotation speed it is possible to better understand the
238 evolution of C_p . Tidal flow velocity, evolving during the trials, changes the turbine rotation speed ω
239 from 20 to 42 rpm. Lower and more stable rotation speed (~ 30 rpm) matches lower velocities, 0.8 - 1.0
240 m/s, and lower C_p . The increase of current velocity to 1.2 m/s leads to increase of rotation speed to 42

241 rpm (TSR ~ 3.6). This speed appears to be optimal for energy production because it allows the
242 turbine's performance to reach its maximum value (0.42).

243 The power curve (Fig. 6b) shows a quasi-linear increase for velocity values ranging from 0.8 to
244 1.05 m/s. A considerable growth of power production is visible for higher velocities. The curve,
245 obtained on the basis of 1-minute averaging, appears quite smooth and contains very few outliers.

246

247 **3.2 Turbulent fluctuations of velocity and power production**

248 Although the power coefficient achieves its optimal value for current velocities above 1.1 m/s, the
249 power production appears unstable and largely intermittent. Fig. 7a clearly shows a higher level of
250 power fluctuations during a longer period of approximately one-hour (14:50-15:50) on November 7.
251 Estimates of the standard deviation of power generated by the turbine, σ_p , is a suitable way to quantify
252 the magnitude of power variability. Fig. 7b shows that σ_p increased more than twice (from 0.05 to 0.12
253 kW) during a short period of test on November 7. Very similar behavior of the output power was
254 found for the other two turbine test runs: on November 8 and 9. Using the quantity σ_p as a measure of
255 the power production intermittency, two characteristic periods are identified in the time history of P :
256 period I, with low σ_p values, and period II when σ_p values were doubled (Fig. 7b, Tab. 1).

257 To identify possible reasons behind such amplification of power fluctuations, ADV velocity time
258 series were analyzed. The velocity evolution on flood flow is given in Fig 8a and compared with the
259 power evolution for the same period (Fig. 7).

260 The level of ambient turbulence in a free tidal stream approaching the turbine, at high Reynolds
261 numbers ($Re \sim 10^6$), is characterized by estimating two quantities: the standard deviation of the
262 velocity, σ , and turbulence intensity, I , both derived from ADV measurements 1 m below the surface,
263 close to the mid-depth of the turbine. 10-minute averaged time series of σ and I , together with two
264 horizontal velocity components (raw data), are presented in Fig. 8.

265 It was specified in section 3.1 that the flow in the Sea Scheldt is almost reversing with a largely
266 dominating streamwise tidal component u . The vertical component of the velocity vector is very small
267 given the low depth on site. On the other hand, v and w fluctuations are also important for turbulence
268 characterization. The ratios of the standard deviations of the spanwise σ_v and vertical component σ_w
269 to the streamwise velocity component σ_u were found to be approximately $\sigma_v/\sigma_u \sim 0.90$ and $\sigma_w/$
270 $\sigma_u \sim 0.63$. The results appeared relatively stable for the whole length of velocity sample and revealed
271 nearly homogeneous turbulence regime in the estuary (for given velocity range). These ratios are 15-
272 20 % higher than that documented by Milne et al. (2013) in the highly energetic tidal flow at the
273 Sound of Islay, UK.

274 The standard deviations σ of velocity, varied approximately in phase with U and with the
275 standard deviation of power, σ_p . The correlation between σ and σ_p is high (0.92) but the relation
276 between two quantities is like a power law function. For the second sub-period, values of σ revealed a

277 large (~50%) increase of turbulent velocity pulsations (Tab. 1). This evolution highlights a significant
278 quantitative change in the flow regime and the ambient turbulence level, in particular when the current
279 velocity exceeds 1 m/s.

280 At the same time, the turbulence intensity did not evolve much, tending towards a mean value $I \sim$
281 0.044 (Fig. 8b and Tab. 1). The correlation between I and σ_p is low (0.44). This suggests that
282 turbulence intensity is unlikely to be the most relevant metric for characterizing the turbulence
283 variability in real tidal flow with continuous velocity evolution. This is the first finding we would like
284 to put forward.

285

286 **3.3 Turbulent properties of the tidal stream and relationship with the output power**

287 A metric conventionally used for quantifying turbulence in a flow is the turbulent kinetic energy
288 which is related to the standard deviation of the velocity as: $TKE = 1/2\sigma^2$. Values of TKE , averaged
289 over two successive sub-periods, show more than 100% increase in turbulent energy for sub-period II
290 (Tab. 1). This highlights a relationship between the level of turbulence (TKE) and the magnitude of
291 power fluctuations, which also doubled.

292 The dissipation rate, ε , is another important indicator used for turbulence characterization. It is
293 associated with turbulent eddies and velocity fluctuations that are not as readily accessible as the
294 global estimation of turbulent kinetic energy. The dissipation rate is quantified through a spectral
295 analysis of velocity time series in the inertial subrange.

296 The PSD of velocity time series recorded by ADV during two successive sub-periods of a tidal
297 cycle is given in Fig. 9. The duration of velocity sample, shown in blue in Fig. 7a, is 1 hour 40 minutes
298 and one hour for the two respective sub-periods. They were chosen to match two typical flow
299 conditions: flood tide with current velocity less than 1 m/s (sub-period I) and more energetic flood
300 flow with velocity ranging from 1 to 1.4 m/s (sub-period II).

301 For each sub-period, the PSD reveals three characteristic frequency subranges: the low frequency
302 subrange ($f < 0.3$ Hz), the inertial subrange ($0.3 \text{ Hz} < f < 2$ Hz), and high frequency subrange ($f > 2$
303 Hz), where the PSD curve is influenced by the noise in the data. Four fundamental properties of the
304 turbulent flow were estimated for each sub-period: the dissipation rate, ε , the integral lengthscale, L ,
305 the Kolmogorov scale, η , and the Taylor-based Reynolds number, Re_λ . The PSD distribution showed
306 good scaling in the inertial subrange for both sub-periods with spectral slope ranging from -1.5 to -1.6.
307 The results are summarized in Tab. 2.

308 A significant difference in turbulent regime was found between periods I and II. The dissipation
309 rate ε doubles when the tidal flow velocity exceeds 1 m/s. This velocity value represents a threshold
310 highlighting a quantitative change in turbulence regime. Tidal stream with velocities larger than 1 m/s
311 has much higher level of ambient turbulence. The PSD distribution (Fig. 9) and the standard deviation
312 of the velocity (Fig. 8b) support this assumption.

313 Estimates of the integral lengthscale L also show large variations with respect to flow conditions.
314 During the flooding tide, the size of the largest (most energetic) eddies increases by a factor of 3.5:
315 from 0.6 m to ~ 2.2 m (Tab. 2). In contrast, the Kolmogorov scale η appears relatively stable during the
316 same period. The smallest eddy size was found to be 0.3 - 0.4 mm which is considered as typical for
317 turbulent river flows or coastal waters.

318 Finally, the Taylor-based Reynolds number Re_λ showed a significant increase, from 500 to 1000,
319 while the mean tidal current speed rose only from 0.9 to 1.2 m/s. This also appears consistent with
320 other estimates documented for different flow conditions in coastal regions (e.g., Luznik et al., 2007).
321 $Re_\lambda \sim 1000$ characterizes highly turbulent flow.

322 Analysis of the scaling properties of velocity time series appears useful for understanding a
323 possible coupling between the turbulence and instantaneous turbine response to velocity fluctuations.
324 Fig. 9b shows the PSD of the power generated on November 7 on flood tide, estimated for each of two
325 sub-periods. The spectra reveal a large difference (more than one decade) in the magnitude of power
326 fluctuations between sub-periods I and II. They also show three characteristic frequency domains. At
327 low frequency ($0.03 < f < 0.3$ Hz), power fluctuations seem to be related with velocity pulsations even
328 if the scaling of the PSD for both quantities is not exactly the same.

329 In the inertial subrange ($0.3 \text{ Hz} < f < 2 \text{ Hz}$), scaling of the PSD distribution of the output power
330 and flow velocity is similar (Fig. 9). Spectral slope is close to $-5/3$ for both quantities: -1.5 for velocity
331 and -1.6 for power. This suggests that in this frequency band, the turbine power appears to be
332 conditioned and probably coupled with the energy cascade in the flow. Fig. 9 also shows that, in this
333 frequency domain, the shape of the power spectrum is largely distorted and reveals that the largest
334 fluctuations of power occur at two frequencies f_0 and $4f_0$, where f_0 denotes the turbine frequency.
335 These frequencies are different for two flow regimes (Fig. 9b grey line). During sub-period I (velocity
336 less than 1 m/s and low power production), the rotation speed of the rotor was found to vary in a range
337 from 20 to 25 rpm, corresponding to f_0 range 0.33 - 0.42 Hz. A large peak of the output power
338 fluctuations occur in this frequency range (Fig. 9b). For sub-period II, characterized by a more
339 energetic flow, the rotation speed of the rotor is close to 40 rpm, providing $f_0 \sim 0.67$ Hz. Strongest
340 variations of power are observed at this frequency. The second harmonic, $4f_0$, corresponds to the blade
341 pass frequency. It refers to the strike when the blade and central shaft are in line with the incident
342 flow. Expression for $4f_0$, given in Li et al., (2014), provides the value of ~ 2.7 Hz, for the mean
343 velocity of 1.2 m/s. The PSD reveals a strong interaction of each of four turbine blades with the
344 incoming flow at this frequency.

345 At high frequencies ($f > 4$ Hz), the output power fluctuations appear to be non-responsive to the
346 dynamics of turbulence in the flow. The PSD for both quantities flattens (Fig. 9) making difficult any
347 evaluation.

348 The fundamental turbulent properties of the flow, estimated from spectral representation of the
349 velocity and summarized in Tab. II, appear to be closely related to the magnitude of power

350 fluctuations. During sub-period II, values of ε , L , and Re_λ are twice higher and correspond to the
351 increase of σ_p from 0.05 to 0.12 kW. However the link between σ_p and the spatial structure of
352 turbulence is not so straightforward. To further investigate a possible relationship between the power
353 fluctuations during flow strengthening and how the turbulence is spatially organized, estimation of the
354 integral lengthscale L was performed for multiple 10-min intervals within two successive sub-periods I
355 and II (two hours in total). The results, shown in Fig. 10, reveal that, for lengthscales $L < 1$ m, the
356 magnitude of the output power fluctuations was relatively low ($\sigma_p \sim 0.04$ kW). As the flow speed
357 increases and approaches the peak speed (~ 1.4 m/s), the size of energy containing eddies also
358 increases (Tab. 2) and the magnitude of power fluctuations become, on average, three times larger (σ_p
359 ~ 0.13 kW). The relationship is linear thus evidencing that the size of energy containing eddies and the
360 level of intermittency of power production are related. In particular, large size turbulent eddies
361 generate large fluctuations of power.

362

363 4. Discussion

364 The present work addressed several issues. First, an estimation of the performance of the Dutch
365 VATT “W2E” was done in continuously evolving tidal flow. During the trials, the optimal conditions
366 for power production were reached when flow speed was approaching 1.2 m/s, providing the highest
367 performance: $C_p \sim 0.4$. However, the power produced in these flow conditions experienced large
368 fluctuations, much larger than for velocity ~ 1 m/s, for example. This kind of intermittency of power
369 production was revealed earlier during device testing in real sea conditions.

370 A number of experimental studies focusing on assessment of the performance of scaled horizontal
371 axis tidal turbines (HATTs) were conducted recently in the Strangford Lough (Northern Ireland) (e.g.,
372 MacEnri et al., 2013; Jeffcoate et al., 2015; Frost et al., 2018). Frost et al. (2018) assessed the
373 performance of a 1.5 m diameter HATT (designed by SCHOTTEL Hydro Ltd) in a real tidal flow and
374 in a towing tank. The laboratory results showed a peak $C_p = 0.44$ in uniform flow, whilst peak
375 performance in the real tidal flow featured a $C_p = 0.38$. The 13% drop in peak power performance
376 between the laboratory and field results was attributed (i) to the Doppler noise, biasing the velocity
377 data recorded by ADCP, and (ii) to the turbulence modifying the flow regime and producing the flow
378 instability. Similar effect was documented by Jeffcoate et al. (2015) during a 1/10 scale Eppler type
379 turbine tests mounted on a moored pontoon in a tidal flow. It was inferred that the performance of the
380 tested turbine was affected by turbulence. At the same time, the results revealed that higher velocity
381 fluctuations in the approaching tidal flow caused higher variations in the rotation speed, torque and
382 power generated by the turbine.

383 The present study aimed to clarify how the turbulence in a tidal flow affects the power
384 production. This raises some specific questions: what is the range of velocity when there are strong
385 interactions with the turbine, what is the dominant response frequency, how large is the response

386 amplitude? We also sought to highlight a relation between a time-dependent structure of the turbulent
387 flow and the magnitude of power fluctuations.

388 Spectral analysis of velocities and the output power fluctuations were used to identify a region in
389 which the turbine power appears to be conditioned by and strongly coupled with the energy cascade in
390 the flow. Such a region corresponds to the inertial subrange (0.3 - 2 Hz) where the PSD distribution
391 follows the Oboukhov-Kolmogorov $k^{-5/3}$ law. This is not a coincidence but a particular indication that
392 there is a relationship between fluctuations of the output power generated by the tidal turbine and
393 turbulence in the flow.

394 Our results showed that in a tidal flow with velocities ranging from 0.8 to 1.4 m/s, the turbulent
395 kinetic energy is cascading from larger eddies of size $L \sim 0.6 - 2$ m to smaller eddies of size less than
396 one mm ($\eta \sim 0.4$ mm) and then dissipates into heat. Values of dissipation ε corresponding to these
397 integral lengthscales are $1.2 \times 10^{-4} \text{ m}^2\text{s}^{-3}$ and $2.4 \times 10^{-4} \text{ m}^2\text{s}^{-3}$ respectively (Tab. 1). The larger the flow
398 speed, the larger the level of velocity pulsations, the turbulent kinetic energy production and
399 dissipation (Pope, 2000).

400 The impact of the level of ambient turbulence on turbine performance in the real flow
401 conditions, is not easy to quantify because all quantities change continuously. Low flow velocities (\sim
402 0.8-1.0 m/s) observed during sub-period I correspond to lower turbulence level ($\varepsilon \sim 1.2 \times 10^{-4} \text{ m}^2\text{s}^{-3}$)
403 and lower C_p values (~ 0.3). Larger velocities, recorded during the peak flood flow (1.1 – 1.4 m/s),
404 generate more turbulence ($\varepsilon \sim 2.4 \times 10^{-4} \text{ m}^2\text{s}^{-3}$) but do not decrease the turbine performance. Another
405 important point is that turbulent properties in natural flow are site dependent and influenced by the
406 flow configuration, bathymetry, nature of the seabed, presence of built infrastructure such as bridges,
407 piers, etc. Therefore, the impact of turbulence on turbine performance will be also site dependent. This
408 makes turbine test results difficult to interpret. In this sense, a comparative study of the turbine
409 performance in a turbulent tidal flow and in calm water using towed platforms (e.g. Jeffcoate, 2015)
410 would be valuable and complementary to experiments in flume tanks where the ratio of lengthscales of
411 turbulent motions, in relation with the size of tested devices, is limited.

412 MacEnri et al. (2013) was the first who performed a comprehensive analysis of the SeaGen
413 performance and demonstrated that standard deviation of the velocity, assumed to be a measure of the
414 turbulence strength, is likely to be one of the significant factors that contributes to flicker level. Large
415 fluctuations of the output power were found at frequency ~ 0.5 Hz which is fundamental (turbine)
416 frequency. Similar results were documented by Frost et al. (2018) for a scaled turbine, tested in the
417 Strangford Lough. Power fluctuations were related to turbulence effect. To the best of our knowledge,
418 results of field experiments published and available for the community to date are far and few. Our
419 experimental results demonstrated a considerable increase in output power fluctuations occurring
420 when velocity exceeds 1 m/s and when the flow regime becomes more turbulent. The frequency f_0 of
421 the largest fluctuations of power changes continuously with respect to the flow speed.

422 A linear relationship between the turbulence lengthscale L and the magnitude of power
423 fluctuation σ_p was established. The correlation was found high (0.96). The use of L allowed to
424 demonstrate how the turbulence is spatially organized and to compare the turbulence lengthscale with
425 the turbine dimensions. In particular, as the size of turbulent eddies matches the turbine size, σ_p
426 exhibits a considerable increase. A quantitative change in interaction between the operating turbine
427 and turbulence is observed at scale $L \sim 1.0 - 1.5$ m (Fig. 10). Large size turbulent eddies exert large
428 loads on the blades, strongly affecting torque and causing large power pulsations. The significance of
429 the effect of turbulence on rotor loads and turbine performance was demonstrated recently by
430 Blackmore et al. (2016) and Chamorro et al. (2013), based on extensive tests of a scaled turbine in a
431 flume tank. Our results confirm their findings and provide further explanation of the interaction
432 between a turbulent flow and a tidal turbine.

433

434 **5. Conclusion**

435 The performance of a Darrieus type tidal turbine of the Dutch company “W2E” was assessed in
436 real sea conditions in the Sea Scheldt. Based on simultaneous output power and velocity
437 measurements, the turbine performance (C_p) was evaluated at different flow regimes, providing the
438 peak value of 0.42 for velocity range 1.15-1.2 m/s. It was shown that turbulent fluctuations of velocity
439 in a tidal flow is the major factor responsible for the intermittency of power production by the turbine.
440 Turbulence intensity I , commonly used by engineers to quantify the level of ambient turbulence, is a
441 metric that in general does not alone capture quantitative changes in the turbulent regime during the
442 tidal flow transition from lower to higher velocities. Other quantities, such as dissipation rate, ϵ , the
443 integral lengthscale, L , and the standard deviation of the velocity appear more appropriate for
444 turbulence characterization. The magnitude of power fluctuations was found to be proportional to L
445 and the strongest impact of turbulence on power generation was detected when the size of highest
446 energy eddies attains and exceeds the turbine size. Our results highlighted that the magnitude of power
447 fluctuations is related to the spatial structure of the turbulence. This finding has important practical
448 implications since it suggests that the design of hydrokinetic turbines needs to take into account the
449 spectral content of turbulence in the approaching flow which could vary significantly from site to site.

450 Our recommendation to the community of engineers involved in tidal energy conversion projects
451 is hence the following: because turbulence is site dependent, ADV measurements should be performed
452 at tidal energy sites prior to turbine testing. High quality data recorded by ADV can help to optimize
453 the design and size of turbines in order to minimize an extra load on the blades which are clearly
454 identified as the prime source of fatigue.

455

456 **Acknowledgments**

457 The authors acknowledge the support of the Interreg IVB (NW Europe) «Pro-Tide» Program. The
458 output power data were kindly provided by Reiner Rijke (Water2Energy). Technical support of

459 Roeland Notele (Seakanal) and experience of Eric Lecuyer (LOG) during the surveys are also
460 acknowledged. The authors wish to thank two anonymous reviewers whose comments on an earlier
461 draft of this manuscript helped in improving the final accepted version.

462

463 **References**

- 464 Bahaj, A. S., Molland, A. F., Chaplin, J. R., & Batten, W. M. J. (2007). Power and thrust
465 measurements of marine current turbines under various hydrodynamic flow conditions in a
466 cavitation tunnel and a towing tank. *Renewable energy*, 32(3), 407-426.
- 467 Bahaj, A. S., & Myers, L. E. (2013). Shaping array design of marine current energy converters through
468 scaled experimental analysis. *Energy*, 59, 83-94.
- 469 Batten W. M. J., Bahaj A. S., Molland A. F., Chaplin J. R. (2008). The prediction of the hydrodynamic
470 performance of marine current turbines. *Renewable Energy*, 33(5), 1085–1096.
- 471 Batten, W. M., Harrison, M. E., & Bahaj, A. S. (2013). Accuracy of the actuator disc-RANS approach
472 for predicting the performance and wake of tidal turbines. *Phil. Trans. R. Soc. A*, 371(1985),
473 20120293.
- 474 Blackmore T., Myers L. E., Bahaj A. S. (2016). Effects of turbulence on tidal turbines: Implications to
475 performance, blade loads, and condition monitoring. *International Journal of Marine Energy*,
476 14:1–26.
- 477 Chamorro L. P., Hill C., Morton S., Ellis C., Arndt R. E. A., Sotiropoulos F. (2013). On the interaction
478 between a turbulent open channel flow and an axial-flow turbine. *Journal of Fluid Mechanics*,
479 716:658–670.
- 480 Churchfield, M. J., Li, Y., Moriarty, P. J. (2013). A large-eddy simulation study of wake propagation
481 and power production in an array of tidal-current turbines. *Phil. Trans. R. Soc. A*, 371(1985),
482 20120421.
- 483 Frish U. (1995). The legacy of A.N. Kolmogorov. Cambridge University Press.
- 484 Goormans, T., Smets, S., Rijke, R. J., Vanderveken, J., Ellison, J., & Notel , R. (2016). In-situ scale
485 testing of current energy converters in the Sea Scheldt, Flanders, Belgium. In *Sustainable*
486 *Hydraulics in the Era of Global Change: Proceedings of the 4th IAHR Europe Congress, Liege,*
487 *Belgium, 27-29 July 2016*. CRC Press (p. 290-297).
- 488 Guerra, M., & Thomson, J. (2017). Turbulence measurements from five-beam acoustic Doppler
489 current profilers. *Journal of Atmospheric and Oceanic Technology*, 34(6), 1267-1284.
- 490 Frost, C., Benson, I., Jeffcoate, P., Els ber, B., & Whittaker, T. (2018). The Effect of Control Strategy
491 on Tidal Stream Turbine Performance in Laboratory and Field Experiments. *Energies*, 11(6), 1533.
- 492 Jeffcoate P., Starzmann R., Elsaesser B., Scholl S., Bischoff S. (2015). Field measurements of a full
493 scale tidal turbine. *International Journal of Marine Energy*, 12:3–20.
- 494 Li, Y., Yi, J., Song, H., Wang, Q., Yang, Z., Kelley, N. and Lee, K. (2014). On natural frequency of
495 tidal power systems-A discussion of sea testing. *Applied Physics Letters*, 105(2), 023902-1-5
- 496 Li, Y., & alısal, S. M. (2010). A discrete vortex method for simulating a stand-alone tidal-current
497 turbine: Modeling and validation. *Journal of Offshore Mechanics and Arctic Engineering*, 132(3),
498 1410-1416.
- 499 Luznik L., Zhu W., Gurka R., Katz J., Nimmo Smith W. A. M., Osborn T. R. (2007). Distribution of
500 energy spectra, Reynolds stresses, turbulence production, and dissipation in a tidally driven bottom
501 boundary layer. *Journal of Physical Oceanography*, 37(6):1527–1550.
- 502 MacEnri J., Reed M., Thiringer T. (2013). Influence of tidal parameters on SeaGen flicker
503 performance. *Philosophical Transactions of the Royal Society of London A: Mathematical,*
504 *Physical and Engineering Sciences*, 371(1985):20120247.

505 McNaughton J., Harper S., Sinclair R., Sellar B. (2015). Measuring and modelling the power curve of
506 a commercial-scale tidal turbine. In *Proceedings of the 11th European Wave and Tidal Energy*
507 *Conference (EWTEC)*, 6-11 Sept 2015, Nantes, France.

508 Medina, O. D., Schmitt, F. G., Calif, R., Germain, G., & Gaurier, B. (2017). Turbulence analysis and
509 multiscale correlations between synchronized flow velocity and marine turbine power production.
510 *Renewable Energy*, 112, 314-327.

511 Milne, I. A., Sharma, R. N., Flay, R. G., & Bickerton, S. (2013). Characteristics of the turbulence in
512 the flow at a tidal stream power site. *Phil. Trans. R. Soc. A*, 371(1985), 20120196.

513 Mycek P., Gaurier B., Germain G., Pinon G., Rivoalen E. (2014). Experimental study of the
514 turbulence intensity effects on marine current turbines behaviour. Part I: One single turbine.
515 *Renewable Energy*, 66:729–746.

516 Neill, S. P., Hashemi, M. R., & Lewis, M. J. (2014). The role of tidal asymmetry in characterizing the
517 tidal energy resource of Orkney. *Renewable Energy*, 68, 337-350.

518 Pinon G., Mycek P., Germain G., Rivoalen E. (2012). Numerical simulation of the wake of marine
519 current turbines with a particle method. *Renewable Energy*, 46:111–126.

520 Pope S. B. (2000). *Turbulent flows*. Cambridge University Press.

521 Richard J.-B., Thomson J., Polagye B., Bard J. (2013). Method for identification of doppler noise
522 levels in turbulent flow measurements dedicated to tidal energy. *Int. Journal of Marine Energy*,
523 3(4):52–64.

524 Tatum, S. C., Frost, C. H., Allmark, M., O’Doherty, D. M., Mason-Jones, A., Prickett, P. W., ... &
525 O’Doherty, T. (2016). Wave–current interaction effects on tidal stream turbine performance and
526 loading characteristics. *International Journal of Marine Energy*, 14, 161-179.

527 Thiébaud, M., & Sentchev, A. (2016). Tidal stream resource assessment in the Dover Strait (eastern
528 English Channel). *International journal of marine energy*, 16, 262-278.

529 Thiébaud, M., & Sentchev, A. (2017). Asymmetry of tidal currents off the W. Brittany coast and
530 assessment of tidal energy resource around the Ushant Island. *Renewable energy*, 105, 735-747.

531 Thomson, J., Polagye, B., Richmond, M., & Durgesh, V. (2010). Quantifying turbulence for tidal
532 power applications. In *OCEANS 2010 MTS/IEEE SEATTLE* (pp. 1-8). IEEE.

533 Thomson J., Polagye B., Durgesh V., Richmond M. C. (2012). Measurements of turbulence at two
534 tidal energy sites in Puget Sound, WA. *Oceanic Engineering, IEEE J. of Oceanic Engineering*,
535 37(3):363–374.

536 Verbeek M., Labeur R., Uijttewaal W., De Haas P. (2017). The near-wake of Horizontal Axis Tidal
537 Turbines in a storm surge barrier. In *Proceedings of the 12th European Wave and Tidal Energy*
538 *Conference*, 27th - 1st Sept. 2017, Cork, Ireland, pages 1179–1–6.

539

540

541 **Tables**

542

543 **Table 1.** Parameters of the flow regime approaching the turbine for two sub-periods of flood tide:
 544 mean horizontal velocity components, standard deviation (s.t.d.) of the current velocity, turbulent
 545 kinetic energy and turbulent intensity. Sub-periods I and II are identified in Fig. 7.

546

Sub-period	Mean velocity (m/s)		s.t.d. of the velocity (m/s) and TKE (m^2/s^2)		Turb. intensity
	$\langle u \rangle$	$\langle v \rangle$	σ	TKE	I
I	0.9	0.1	0.065	0.002	0.041
II	1.25	0.15	0.102	0.005	0.047

547

548

549 **Table 2.** Turbulent properties of the tidal flow approaching the turbine for two characteristic sub-
 550 periods (I and II) of flood tide: dissipation rate ε of the turbulent kinetic energy, integral lengthscale L ,
 551 Kolmogorov scale η , Taylor based Reynolds number Re_λ , and spectral slope s .

552

Turbulent properties	$\varepsilon(m^2s^{-3})$	$L(m)$	$\eta(mm)$	Re_λ	s
Sub-period I	1.2×10^{-4}	0.6	0.4	492	-1.6
Sub-period II	2.3×10^{-4}	2.2	0.3	1073	-1.5

553

554

555 **Figure captions**

556 **Fig. 1.** Upper panel: Darrieus type tidal turbine of the Dutch company Water2Energy mounted on a
557 surface floating platform for trials in the Sea Scheldt, in autumn 2014.

558 Lower panel: Experimental pontoon installed in the tidal estuary (the Sea Scheldt) for tidal turbine
559 tests in real sea conditions. Velocity measurements were performed by ADCP and ADV installed on a
560 steel beam extending out from the side of the pontoon and positioned upstream in front of the turbine
561 (inset in lower panel).

562 **Fig. 2.** Arian view of the test site location in the Sea Scheldt. The pontoon and turbine locations are
563 shown in white within the red circle close to the bridge (Temse bridge). Flood flow direction is given
564 in white and the orthogonal frame, used for projection of current velocity components, is given in
565 black.

566 **Fig. 3.** Tidal current ellipse on site derived from ADCP velocity measurements averaged in the surface
567 layer 2-m thick. Red and blue points indicate 1-min averaged current velocities during flood and ebb
568 tide respectively. Black crosses show the mean flood and ebb flow velocity values.

569 **Fig. 4.** (a) Ten minutes averaged velocity time series measured by ADCP at 0.8 m depth in November
570 2014 during the trials. Flood and ebb tide velocities are shown in red and blue respectively. Solid and
571 dashed lines show the streamwise (u) and spanwise (v) velocity components. (b) Power generated by
572 the turbine on flood flow during the same period. Power records shown by shading were used for
573 turbine performance assessment.

574 **Fig. 5.** Current velocity profiles (1-minute averaged) derived from ADCP measurements during two-
575 hour period on November 7, 2014 14:00 – 16:00 (UTC). Color matches the depth-average velocity.

576 **Fig. 6.** Performance coefficient C_p as a function of flow velocity (a) and the power curve of the tidal
577 turbine “W2E” (b). The output power and velocity are one-minute averaged (grey dots). Standard
578 deviations (red dashed lines) are estimated within the velocity intervals of 0.05 m/s.

579 **Fig. 7.** (a) Power generated by the “W2E” tidal turbine during the test run on November 7, 2014. One
580 second averaged time series of the power recorded at 100 Hz is given in black. One minute averaged
581 power is given in grey. (b) Standard deviation of power fluctuations estimated within 10-min intervals.
582 Periods of moderate and high fluctuations of the output power, denoted by I and II, are shown in light
583 and dark blue respectively.

584 **Fig. 8.** (a) Current velocity time series (raw data) recorded by ADV at 16 Hz during flood tide on
585 November 7, 2014. Streamwise velocity component u is shown in blue, spanwise component v in grey.
586 Light grey line shows the mean (low-pass filtered) velocity. Black dots represent the ADCP velocities
587 at 0.8 m depth and averaged within 10-min intervals. (b) Evolution of the turbulence intensity (I) and
588 the standard deviation of current velocity (σ) during the same period. Light and dark blue match sub-
589 periods of lower and larger velocity variations and numbered I and II in (a).

590 **Fig. 9.** (a) Power Spectral Density (PSD) of the current velocity recorded by ADV (streamwise
591 component) in the approaching flow during two specific sub-periods I and II on flood tide, identified
592 in Fig. 7a. Red dashed line shows the spectral slope $f^{-5/3}$. Grey dashed lines show the best fit of the
593 spectral slope in the inertial subrange.

594 (b) PSD of the output power generated by the turbine on November 7, 2014, during sub-periods I and
595 II on flood flow. Red line shows the spectral slope $f^{-5/3}$. The mean frequency of turbine rotation is
596 shown by f_0 for each sub-period. The second harmonic, $4f_0$, matches the blade pass frequency.

597 **Fig. 10.** The standard deviation of output power fluctuations σ_p versus the integral lengthscale L , both
598 estimated over six successive 10-minute intervals of sub-periods I and II.

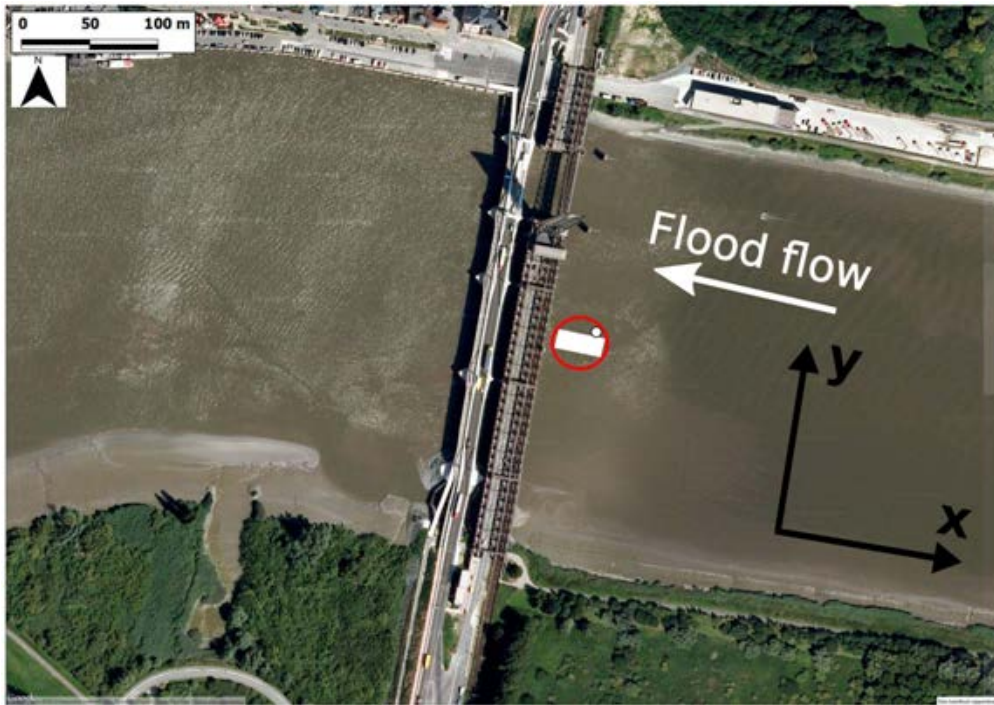
599

600 **Figures**
601



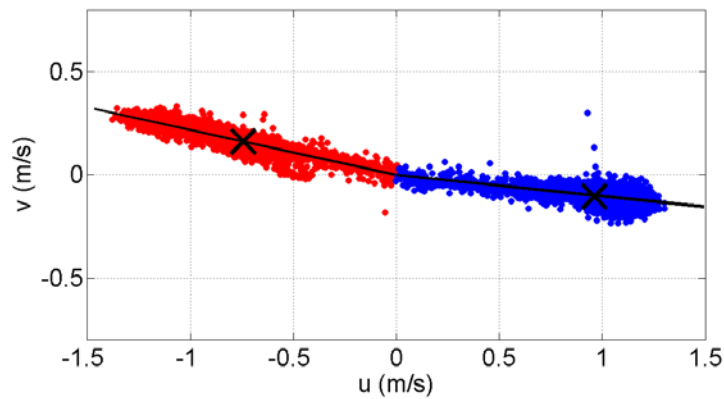
602
603 **Fig. 1.** Upper panel: Darrieus type tidal turbine of the Dutch company Water2Energy mounted on a
604 surface floating platform for trials in the Sea Scheldt, in autumn 2014.
605 Lower panel: Experimental pontoon installed in the tidal estuary (the Sea Scheldt) for tidal turbine
606 tests in real sea conditions. Velocity measurements were performed by ADCP and ADV installed on a
607 steel beam extending out from the side of the pontoon and positioned upstream in front of the turbine
608 (inset in lower panel).
609

610



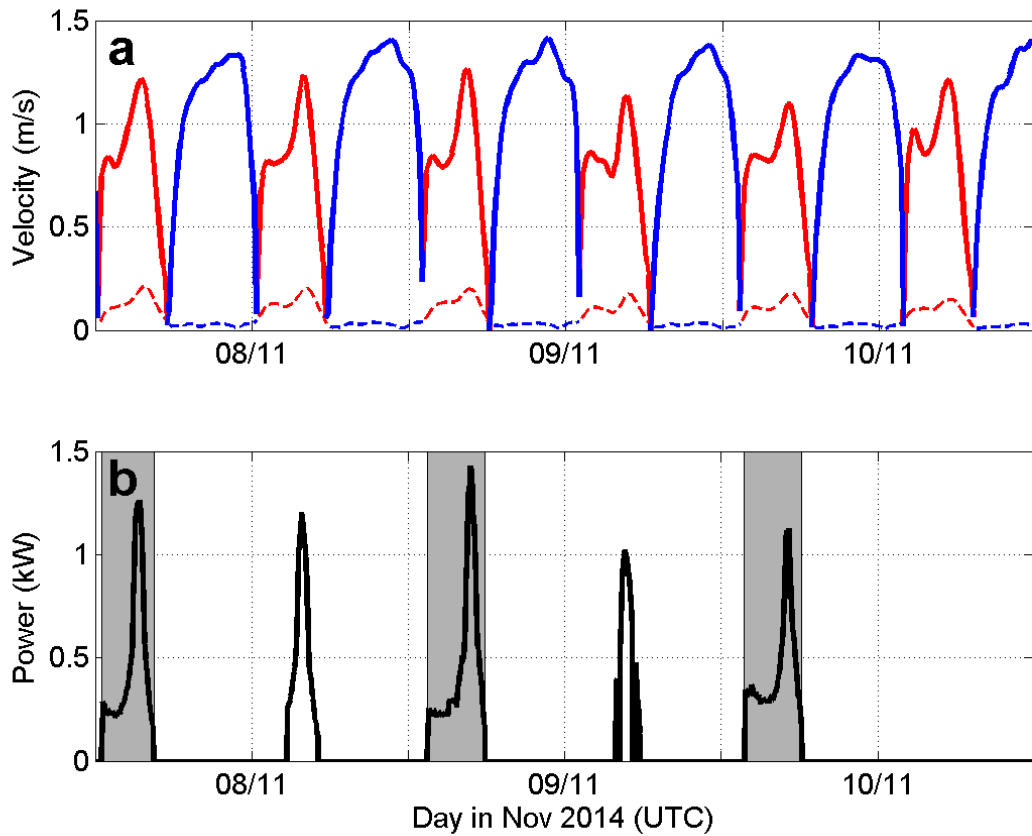
611
612
613
614
615
616
617
618

Fig. 2. Arian view of the test site location in the Sea Scheldt. The pontoon and turbine locations are shown in white within the red circle close to the bridge (Temse bridge). Flood flow direction is given in white and the orthogonal frame, used for projection of current velocity components, is given in black.



619
620
621
622
623
624

Fig. 3. Tidal current ellipse on site derived from ADCP velocity measurements averaged in the surface layer 2-m thick. Red and blue points indicate 1-min averaged current velocities during flood and ebb tide respectively. Black crosses show the mean flood and ebb flow velocity values.

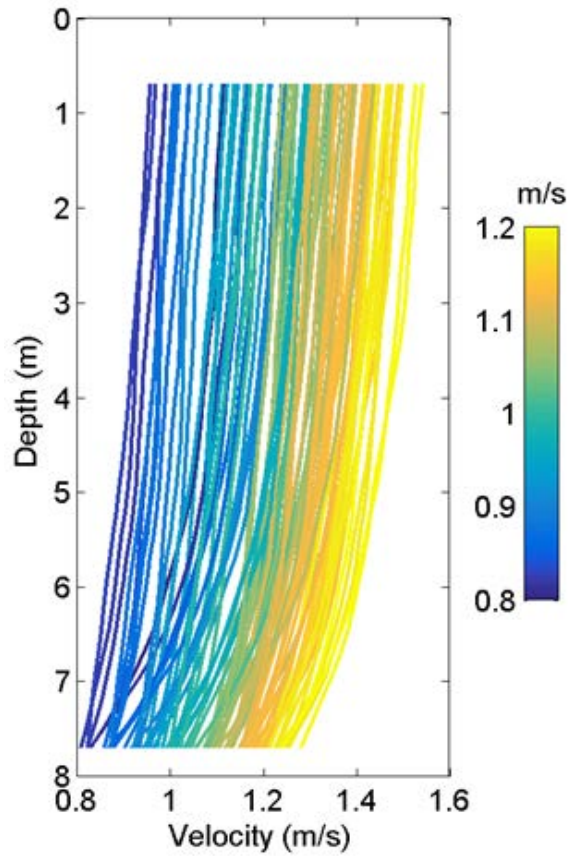


626

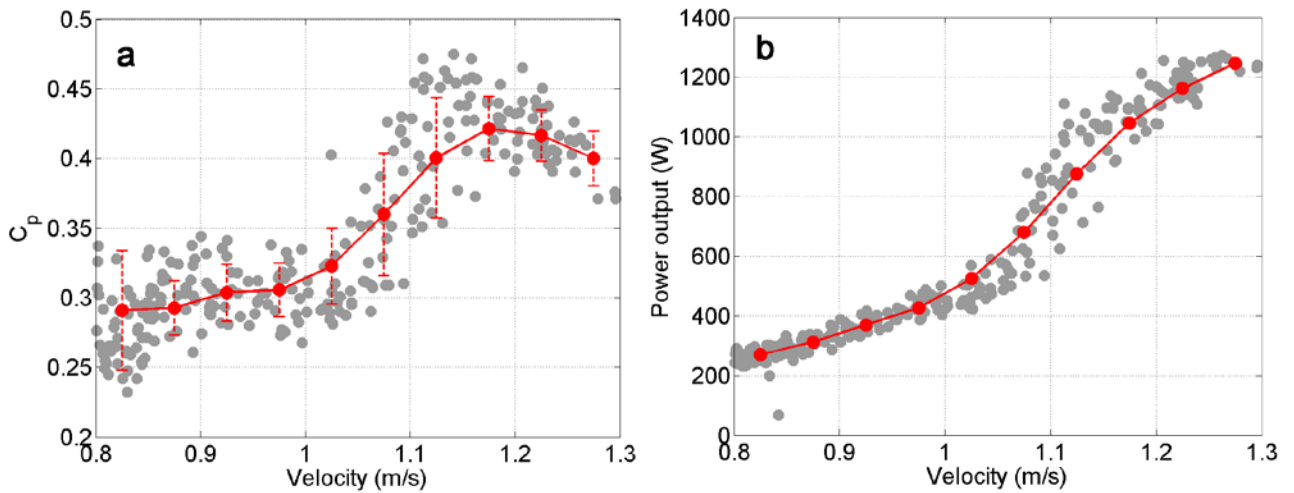
627 **Fig. 4.** (a) Ten minutes averaged velocity time series measured by ADCP at 0.8 m depth in November
 628 2014 during the trials. Flood and ebb tide velocities are shown in red and blue respectively. Solid and
 629 dashed lines show the streamwise (u) and spanwise (v) velocity components.

630 (b) Power generated by the turbine on flood flow during the same period. Power records shown by
 631 shading were used for turbine performance assessment.

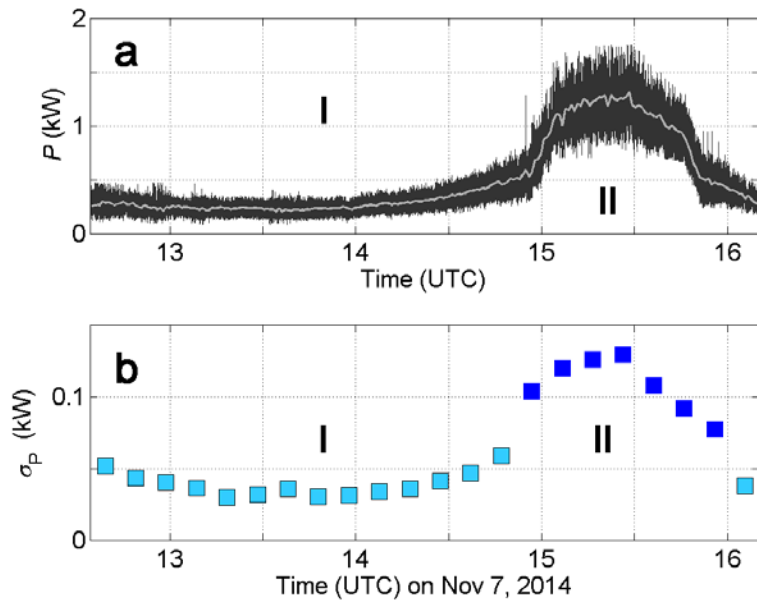
632



633
 634 **Fig. 5.** Current velocity profiles (1-minute averaged) derived from ADCP measurements during two-
 635 hour period on November 7, 2014 14:00 – 16:00 (UTC). Color matches the depth-average velocity.
 636
 637

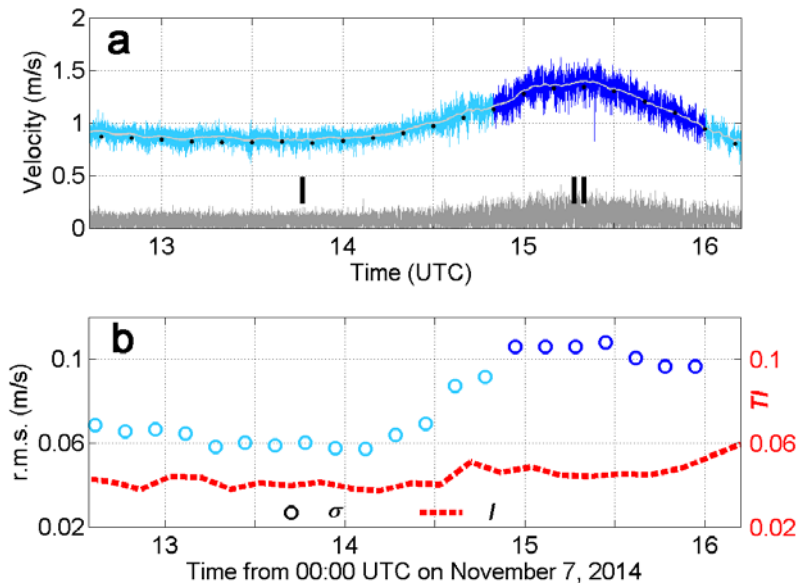


638
 639
 640 **Fig. 6.** Performance coefficient C_p as a function of flow velocity (a) and the power curve of the tidal
 641 turbine “W2E” (b). The output power and velocity are one-minute averaged (grey dots). Standard
 642 deviations (red dashed lines) are estimated within the velocity intervals of 0.05 m/s.
 643



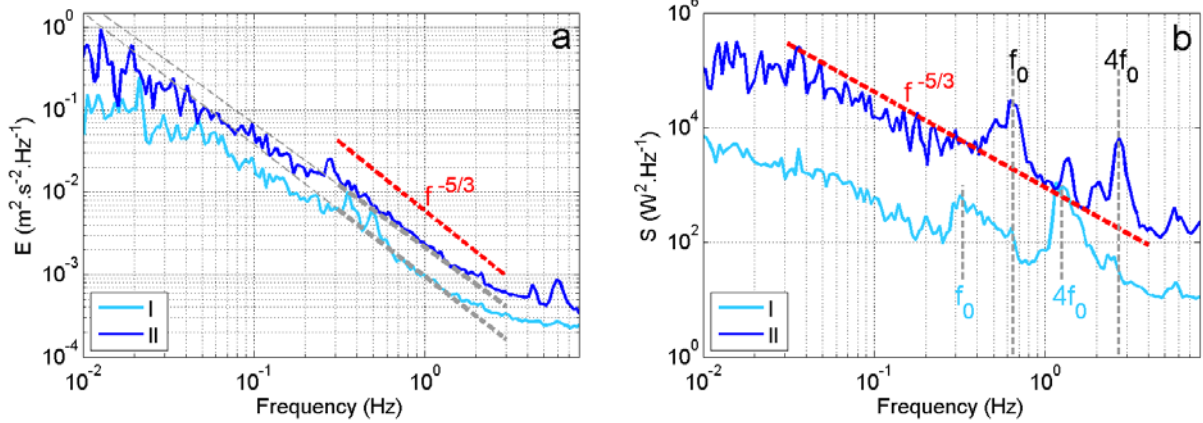
645

646 **Fig. 7.** (a) Power generated by the “W2E” tidal turbine during the test run on November 7, 2014. One
 647 second averaged time series of the power recorded at 100 Hz is given in black. One minute averaged
 648 power is given in grey. (b) Standard deviation of power fluctuations estimated within 10-min intervals.
 649 Periods of moderate and high fluctuations of the output power, denoted by I and II, are shown in light
 650 and dark blue respectively.

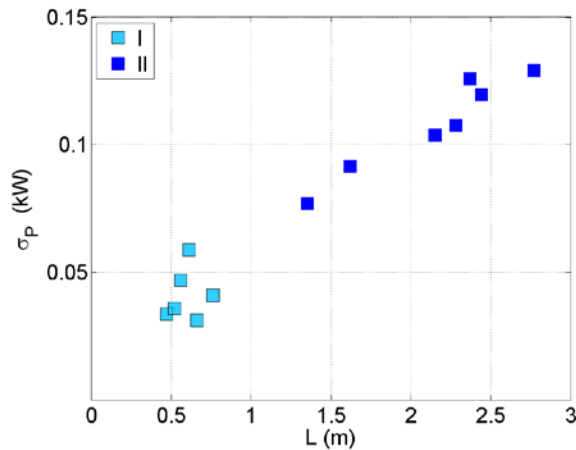


651

652 **Fig. 8.** (a) Current velocity time series (raw data) recorded by ADV at 16 Hz during flood tide on
 653 November 7, 2014. Streamwise velocity component u is shown in blue, spanwise component v in grey.
 654 Light grey line shows the mean (low-pass filtered) velocity. Black dots represent the ADCP velocities
 655 at 0.8 m depth and averaged within 10-min intervals. (b) Evolution of the turbulence intensity (I) and
 656 the standard deviation of current velocity (σ) during the same period. Light and dark blue match sub-
 657 periods of lower and larger velocity variations and numbered I and II in (a).



658
 659 **Fig. 9.** (a) Power Spectral Density (PSD) of the current velocity recorded by ADV (streamwise
 660 component) in the approaching flow during two specific sub-periods I and II on flood tide, identified
 661 in Fig. 7a. Red dashed line shows the spectral slope $f^{-5/3}$. Grey dashed lines show the best fit of the
 662 spectral slope in the inertial subrange.
 663 (b) PSD of the output power generated by the turbine on November 7, 2014, during sub-periods I and
 664 II on flood flow. Red line shows the spectral slope $f^{-5/3}$. The mean frequency of turbine rotation is
 665 shown by f_0 for each sub-period. The second harmonic, $4f_0$, matches the blade pass frequency.
 666



667
 668 **Fig. 10.** The standard deviation of output power fluctuations σ_P versus the integral lengthscale L , both
 669 estimated over six successive 10-minute intervals of sub-periods I and II.
 670